Available online at www.sciencedirect.com
ScienceDirect
International Journal of Multiphase Flow 34 (2008) 375–392
International Journal of Multiphase Flow
www.elsevier.com/locate/ijmulflow

Effect of inertia on the hydrodynamic interaction between two liquid capsules in simple shear flow

Sai K. Doddi, Prosenjit Bagchi *

Department of Mechanical and Aerospace Engineering, Rutgers University, The State University of New Jersey, 98 Brett Road, Piscataway, NJ 08854, USA

Received 8 May 2007; received in revised form 10 September 2007

Abstract

Three-dimensional numerical simulations using front-tracking method are performed to study the hydrodynamic interaction between two liquid capsules suspended in simple shear flow in presence of inertia. Capsules are modeled as liquid drops surrounded by neo-Hookean elastic membranes. In the limit of zero inertia, it has been known from past research that the hydrodynamic interaction between two deformable particles (drops/capsules) suspended in shear flow results in an irreversible shift in the trajectories of the particles as one particle rolls over the other. In this article, we show that the presence of inertia can significantly alter the capsule trajectories. When inertia is small but finite, the capsules do undergo an irreversible displacement, but the lateral separation between them first decreases before they roll over each other, unlike in $Re \ll 1$. For moderate to high inertia, the capsules reverse their directions of motion before coming close to each other. The reversal of motion occurs progressively earlier in time (that is, the capsules come less closer to each other) with increasing inertia. The long-time behavior of the capsule–capsule interaction at finite inertia showed that the capsules engage in spiraling motions. Based on our simulations, four different regimes of capsule–capsule interaction at finite inertia are identified: (i) a self-diffusive type interaction, (ii) an outwardly spiraling motion, (iii) a fixed-orbit spiraling motion, and (iv) an inwardly spiraling motion in which the capsules settle with zero relative velocity. The reversal of motion, and the spiraling trajectories at finite inertia have no analogy in the limit of zero inertia. Such motions are explained by analyzing the flow field around a deformed capsule which shows reverse flow regions and off-surface stagnation points, similar to those previously reported in case of rigid spheres and cylinders under torque-free condition.

Keywords: Deformable particles/drops/capsules; Numerical simulation; Particle–particle interaction

1. Introduction

Capsules are liquid drops surrounded by thin elastic membranes. Many biological cells including red blood cells are often modeled as capsules (Pozrikidis, 2003). Artificial capsules are also abundant in industrial applications (Borhan and Gupta, 2003; Gutcho, 1979). When placed in a shear flow, a capsule deforms and aligns itself with the flow, as does a liquid drop (Chang and Olbricht, 1993; Pozrikidis, 1995; Barthes-Biesel, 1980). However, there are important differences between a liquid drop and a capsule. For example, in a linear shear flow, a capsule often exhibits a tank-treading motion or a tumbling motion. Deformation of the capsule is governed by the properties of the membrane material, such as, shear, extensional and bending moduli, rather than surface tension. In case of liquid drops, hydrodynamic interaction between a pair of them may result into coalescence, or breakup leading to formation of smaller and satellite drops. In case of capsules, the presence of the membrane prevents them from coalescing.

Dynamics of single capsule has been a subject of investigation for several decades. Deformation of a capsule suspended in a shear flow was measured by Chang and Olbricht (1993). Recently, Risso et al. (2006) experimentally investigated single-file motion of artificial capsules

* Corresponding author.
E-mail address: pbagchi@jove.rutgers.edu (P. Bagchi).

0301-9322/$ - see front matter © 2007 Elsevier Ltd. All rights reserved.
doi:10.1016/j.ijmultiphaseflow.2007.10.011

flowing through narrow tubes. Barthes-Biesel and co-workers (Barthes-Biesel, 1980; Barthes-Biesel and Rallison, 1981; Barthes-Biesel and Sgaier, 1985) developed the theory of small deformation of a capsule suspended in a shear (or, a general linear) flow. Li et al. (1988) computed axisymmetric large deformation of capsules in a straining flow, and Leyrat-Maurin and Barthes-Biesel (1994) studied axisymmetric large deformation of a capsule during its passage through a hyperbolic constriction. Queguiner and Barthes-Biesel (1997) studied the axisymmetric motion of capsules through cylindrical tubes. Pozrikidis (1995) and Ramanujan and Pozrikidis (1998) used boundary integral simulation to consider large deformation of capsules in shear flow. Pozrikidis (2001) and Kwak and Pozrikidis (2001) have also studied the effect of membrane bending resistance on the deformation of a capsule suspended in shear flow and in axisymmetric straining flow. Effect of membrane viscosity on the dynamic response of a capsule was studied by Diaz et al. (2000, 2001). Capsule deformation under various constitutive laws for the membrane material was studied by Barthes-Biesel et al. (2002) and Lac et al. (2004). Effect of membrane pre-stress was studied by Lac and Barthes-Biesel (2005).

While the theory of the dynamics of single capsule has advanced significantly, that of the motion of an ensemble of capsules is still lacking. Barthes-Biesel and Chim (1981) studied the rheology of a dilute suspension of capsules at small deformation. Breyiannis and Pozrikidis (2000) considered suspension of two-dimensional capsules in shear flow.

As a first step towards a comprehensive understanding of capsule suspension, Lac et al. (2007) studied interaction between a pair of capsules in shear flow. The capsules were released with different velocities, and thus they eventually roll over each other. The interaction results in an irreversible shift in trajectory of the capsules. Similar phenomenon has been observed during interaction of liquid drops. Three-dimensional simulation of Loewenberg and Hinch (1997), two-dimensional simulation by Charles and Pozrikidis (1998), and experimental study by Guido and Simeone (1998) showed that the hydrodynamic interaction between a pair of liquid drops suspended in a shear flow with different velocities resulted in an irreversible shift in the drop trajectory. In case of a suspension of many drops/capsules, such irreversible displacement dueto binary interactions collectively leads to the so-called shear-induced self-diffusion which plays an important role in mixing and microstructural evolution of a suspension.

Shear-induced self-diffusion has been mostly studied in the case of suspension of rigid spherical particles. Batchelor and Green (1972) studied the interaction between two rigid spheres in a linear flow, and showed that the trajectories of one sphere relative to the other could be closed (i.e. they do not extend to infinity). The existence of closed trajectories for a pair of spheres was experimentally observed by Darabaner and Mason (1967). If the spheres are perfectly smooth, interaction between a pair of them does not lead to self-diffusion. Self-diffusion of rigid spheres is possible when more than two spheres are present (Acrivos et al., 1992; Wang et al., 1996), or surface roughness is introduced (daCunha and Hinch, 1996). Experimental measurements on shear-induced self-diffusion of rigid particles have been obtained by Eckstein et al. (1977), Leighton and Acrivos (1987), Chang and Powell (1994), and Breedveld et al. (1998, 2001). Theoretical and numerical studies on shear-induced diffusion of rigid particles have been considered by Brady and Bossis (1985), Brady and Morris (1997), Foss and Brady (1999), Marchioro and Acrivos (2001), Drazer et al. (2002), and Sierou and Brady (2004).

The works mentioned above are all in the limit of Stokes flow. The presence of inertia is expected to affect the interaction between a pair of liquid drops/capsules/rigid spheres, as well as the shear-induced diffusion mechanism. Interaction between a pair of liquid drops in presence of inertia has been extensively studied. These studies are complicated by the fact that the drops often coalesce or break upon interaction at high inertia. Depending on the nature of the coalescence and breakup, various regimes of collision can be identified. Here we avoid the discussion on drop–drop collision, and refer to some recent papers by, for example, Pigeonneau and Feuillebois (2002), Qian and Law (1997), Wang et al. (1994), Ashgriz and Poo (1990), Nobari and Tryggvason (1996), Brenn and Kolobaric (2006), Pan and Suga (2005), and Roisman (2004), among others, which give excellent accounts on the subject. We note, however, that the shear-induced diffusion process for non-coalescing and non-breaking liquid drops *in presence of inertia* has not been studied. So is the case for liquid capsules. As for rigid particles, Kromkamp et al. (2005) studied pairwise interaction between two circular particles in a shear flow at finite but small inertia. Kromkamp et al. (2005) observed that though the shear-induced vdiffusion mechanism is present, the trajectories of the particles showed markedly different behavior in presence of inertia.

It appears, therefore, that hydrodynamic interaction between three-dimensional deformable particles *in presence of inertia* lack sufficient investigation. In this paper we address hydrodynamic interaction between two liquid capsules suspended in a linear shear flow in presence of inertia. We choose capsules because unlike liquid drops, they do not coalesce or break upon interaction, and hence provide a 'cleaner' system. At the same time, capsules are deformable like liquid drops. Thus, unlike a pair of smooth rigid spheres which does not show irreversible trajectory shift, a pair of capsules is expected to show this mechanism. As mentioned above, the only study that addressed hydrodynamic interaction of a capsule-pair is the one by Lac et al. (2007) in the limit of zero inertia. Here we extend their study to finite inertia. While inertia is not important for biological applications, it is often relevant for artificial capsules in industrial processes related to food and polymer processing (Borhan and Gupta, 2003).

In this paper we present three-dimensional numerical simulation on capsule dynamics using immersed boundary/front-tracking method. The main objective of the paper is to study the interaction between two capsules in presence of inertia. However, we note that there is virtually no study that addressed the effect of inertia on single capsule dynamics. Therefore, in the first part of the paper, we briefly consider the dynamics of a single capsule suspended in a shear flow in presence of inertia. This is followed by the results on the effect of inertia on capsule–capsule interaction.

2. Flow configuration and simulation technique

The flow configuration is described in Fig. 1. We consider deformation of a capsule, and interaction between two capsules, suspended in a simple (linear) shear flow given by $\mathbf{U} = \{Gy, 0, 0\}$, where G is the shear rate. The initial undeformed shape of a capsule is spherical with diameter a. The fluid, both inside and outside of the capsules, is incompressible and Newtonian. The channel is periodic in the streamwise (x) direction, and in the z-direction. In the y-direction, the flow is bounded by two no-slip walls separated by a distance H. The computational domain is a cube of sides of length H. In the present computation, we take $a/H = 0.16$.

The simulation technique considered here is the front-tracking/immersed boundary method (Unverdi and Tryggvason, 1992) for multiple fluids with different properties. The main idea of the front-tracking method is to use a single set of equations for both the fluids, inside and outside of the capsule. The interface (i.e. the capsule membrane) is accounted for by introducing a body force $\mathbf{F}(\mathbf{x}, t)$ in the governing equations. It is zero everywhere in the flow except at the interface:

$$\mathbf{F}(\mathbf{x}, t) = \int_{\partial S} \mathbf{f}(\mathbf{x}', t)\delta(\mathbf{x} - \mathbf{x}')\,\mathrm{d}\mathbf{x}', \tag{1}$$

where $\mathbf{x}$ is the location of an arbitrary point in the flow domain, $\mathbf{x}'$ is any point on the interface, ∂S is the entire interface, and δ is the three-dimensional Delta function which vanishes everywhere except at the interface. Here $\mathbf{f}$ is the elastic force generated in the membrane due to deformation of the capsule. For incompressible fluids of different viscosities, the governing equations are:

$$\nabla \cdot \mathbf{u} = 0, \quad \text{and} \quad \rho\left[\frac{\partial \mathbf{u}}{\partial t} + \mathbf{u} \cdot \nabla \mathbf{u}\right] = -\nabla p + \nabla \cdot \boldsymbol{\tau} + \mathbf{F}. \tag{2}$$

Here $\mathbf{u}(\mathbf{x}, t)$ is the fluid velocity, ρ is the density, p pressure, and

$$\boldsymbol{\tau} = \mu(\nabla \mathbf{u} + (\nabla \mathbf{u})^{\mathrm{T}}) \tag{3}$$

is the viscous stress tensor. Here $\mu(\mathbf{x}, t)$ is the viscosity in the entire fluid: within a capsule, $\mu = \mu_c$, and for any point outside, $\mu = \mu_0$. As the capsules move and deform, $\mu(\mathbf{x}, t)$ needs to be updated. Following Unverdi and Tryggvason, 1992, this is done by solving a Poisson equation for an indicator function $I(\mathbf{x})$ defined as

$$\mu(\mathbf{x}) = \mu_0 + (\mu_c - \mu_0)I(\mathbf{x}). \tag{4}$$

The governing equations for the fluid flow are solved on a fixed Eulerian grid, and the capsule membrane is tracked in a Lagrangian manner by a set of marker points. Once the fluid velocity is known, the velocity and the new position of the interface is computed as

$$\mathbf{u}(\mathbf{x}') = \int_S \mathbf{u}(\mathbf{x})\delta(\mathbf{x} - \mathbf{x}')\,\mathrm{d}\mathbf{x}, \quad \text{and} \quad \frac{\mathrm{d}\mathbf{x}'}{\mathrm{d}t} = \mathbf{u}(\mathbf{x}'), \tag{5}$$

where S indicates the entire flow domain.

The δ function used in Eqs. (1) and (5) is constructed by multiplying three 1D δ functions as

$$\delta(\mathbf{x} - \mathbf{x}') = \delta(x - x')\delta(y - y')\delta(z - z'). \tag{6}$$

For numerical implementation, a smooth representation of the δ-function is used as

$$\begin{aligned} D(\mathbf{x} - \mathbf{x}') &= \frac{1}{64\Delta^3}\prod_{i=1}^{3}\left(1 + \cos\frac{\pi}{2\Delta}(x_i - x_i')\right) \\ &\quad \text{for } |x_i - x_i'| \leqslant 2\Delta, \quad i = 1, 2, 3, \\ D(\mathbf{x} - \mathbf{x}') &= 0 \quad \text{otherwise}, \end{aligned} \tag{7}$$

where Δ is the Eulerian grid size (Unverdi and Tryggvason, 1992). In discrete form, the integrals in Eqs. (1) and (5) can be written as

$$\mathbf{F}(\mathbf{x}_j) = \Sigma_i D(\mathbf{x}_j - \mathbf{x}_i')\mathbf{f}(\mathbf{x}_i'), \tag{8}$$

$$\mathbf{u}(\mathbf{x}_i') = \Sigma_j D(\mathbf{x}_j - \mathbf{x}_i')\mathbf{u}(\mathbf{x}_j), \tag{9}$$

where i and j represent Lagrangian and Eulerian points, respectively.

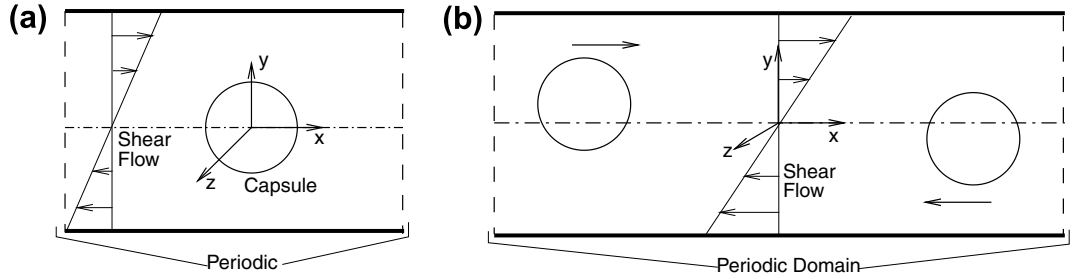

Fig. 1. Schematic of the initial configuration and location of the capsule in shear flow: (a) single capsule, (b) a pair of capsules.

Computation of $\mathbf{f}(\mathbf{x}', t)$ requires a constitutive law for the material of the membrane. Here we assume that the membrane follows the neo-Hookean law. The strain energy function for a neo-Hookean membrane is given by

$$W = \frac{Eh}{6}(\epsilon_1^2 + \epsilon_2^2 + \epsilon_1^{-2}\epsilon_2^{-2} - 3), \tag{10}$$

where ϵ_1 and ϵ_2 are the principal strains, E is the elastic modulus, and h is the membrane thickness. The membrane is discretized using triangular elements. Then $\mathbf{f}$ is obtained at three nodes of each element by differentiating W with respect to the nodal displacement $\mathbf{v}$ (Charrier et al., 1989) as

$$\mathbf{f} = \frac{\partial W}{\partial \epsilon_1}\frac{\partial \epsilon_1}{\partial \mathbf{v}} + \frac{\partial W}{\partial \epsilon_2}\frac{\partial \epsilon_2}{\partial \mathbf{v}}. \tag{11}$$

The main idea is that a general 3D deformation of the membrane can be reduced to a 2D problem by assuming that individual triangular element on the membrane remains flat even after deformation, and that the membrane force remains invariant under a coordinate transformation. This assumption still allows large deformation of the capsule. The resultant force $\mathbf{f}$ at a membrane node is the vector sum of the forces exerted by all elements surrounding that node. The method has been used earlier in a separate code

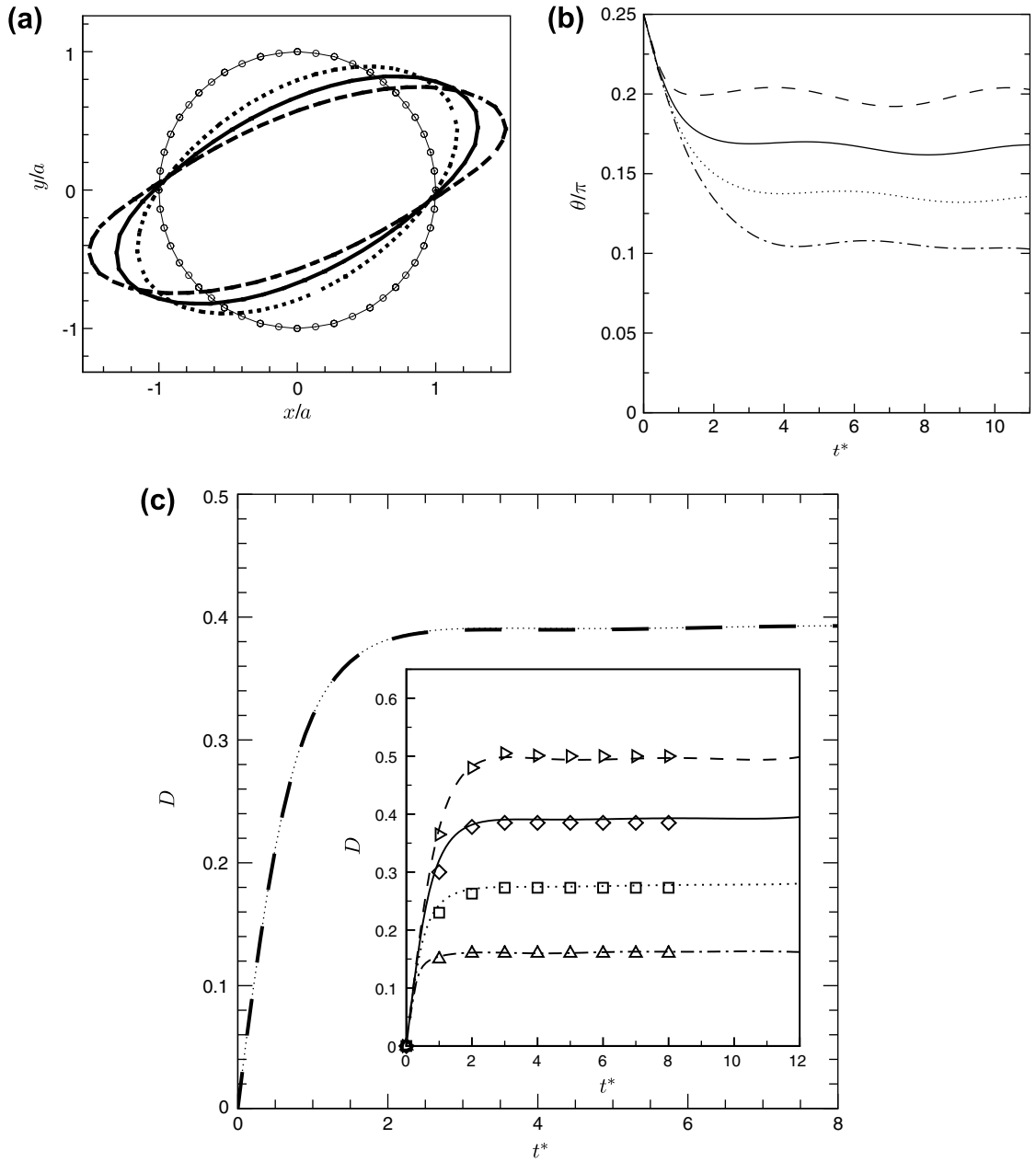

Fig. 2. Deformation of single capsule at $Re \ll 1$ in shear flow. (a) Steady-state shapes of deformed capsules (shown in x–y plane); the initial capsule shape is shown by —○—. (b) Angular orientation θ w.r.t. x-axis. Line patterns for (a) and (b) are as follows: –·–· $Ca = 0.025$; ··· $Ca = 0.05$, — $Ca = 0.1$, - - - $Ca = 0.2$. (c) Deformation parameter D. Resolution test using 80^3 (—) and 120^3 (···) Eulerian points is shown. Inset: comparison with Ramanujan and Pozrikidis (1998). Symbols are the results from Ramanujan and Pozrikidis, lines are from present simulation. Line patterns are for various Ca as in (b).

by Eggleton and Popel (1998) and validated against the analytical results for small deformation of capsules.

The governing equations are made dimensionless using a as the characteristic length scale, and the inverse shear rate G^{-1} as the time scale. The dimensionless time $t\ G^{-1}$ is denoted by t^*. The major dimensionless parameters are the Capillary number $Ca = \mu Ga/Eh$ which is the ratio of the viscous stress to the elastic force of the capsule membrane, and the Reynolds number $Re = \rho Ga^2/\mu$. In the limit of small inertia, capillary number is the relevant parameter, whereas at finite inertia it is customary to use the Weber number $We = ReCa = \rho G^2 a^3/Eh$ instead of the capillary number. The viscosities of the capsule liquid and the exterior liquid are the same.

The governing equations are discretized spatially using a second-order finite difference scheme, and temporally using a two-step time-split scheme. In this method the momentum equation is split into an advection–diffusion equation and a Poisson equation for the pressure. The nonlinear term in the advection–diffusion equation is treated explicitly using a second–order Adams–Bashforth scheme, and the viscous terms are treated implicitly using the Crank–Nicholson scheme. The advection–diffusion equation is solved using an ADI (alternating direction implicit) scheme. The velocity is not divergence-free at the end of the advection–diffusion step. The Poisson equation is then solved to obtain pressure at the next time level. Using the new pressure, the velocity is corrected to make it divergence-free. In order to reduce computation, the Poisson equation is Fourier transformed in the x-direction yielding a set of 2D decoupled PDEs which is directly inverted to obtain pressure. Typical resolutions used in this study are: $120 \times 120 \times 120$ Eulerian points, 1280 triangular elements on capsule surface (Lagrangian mesh), and dimensionless timestep $\sim 10^{-3}$.

3. Results and discussion

3.1. Validation: capsule deformation at $Re \ll 1$

We first validate the front-tracking methodology by considering large deformation of a spherical capsule at

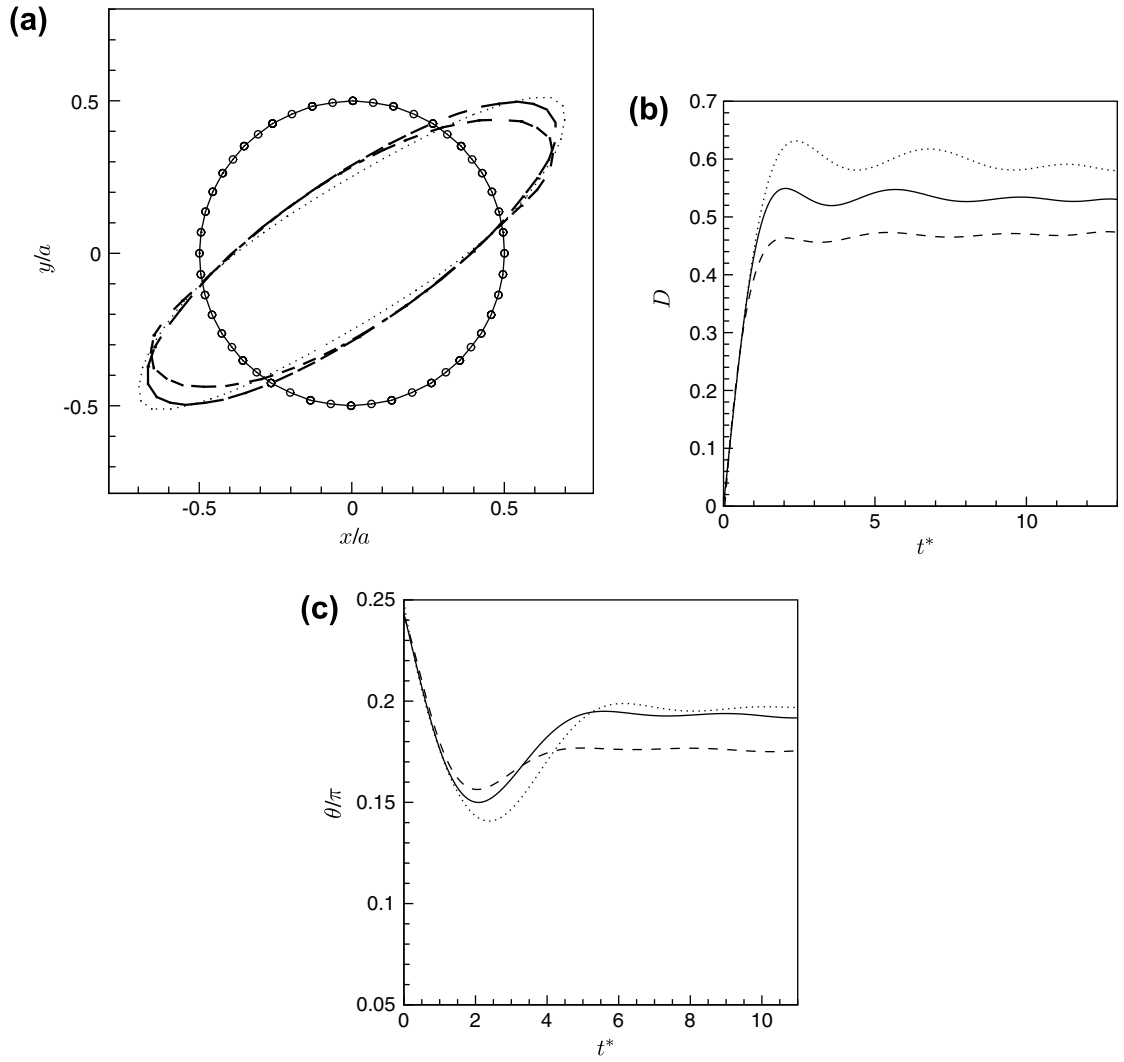

Fig. 3. Deformation of single capsule at finite Re. (a) Steady shapes, (b) deformation parameter D, and (c) angular orientation θ. Line patterns are: --- Re= 10; — $Re = 25$; $\cdots$ $Re = 50$ ($We = 2$, 5, 10, respectively). In (a), the initial capsule shape is shown by —○—.

low Reynolds numbers ($Re \ll 1$) suspended in simple shear flow. When placed in a shear flow, a capsule deforms and aligns itself with the flow (Chang and Olbricht, 1993; Pozrikidis, 1995; Barthes-Biesel, 1980). Previous investigators have studied large deformation of capsules in the limit of $Re \ll 1$ using boundary integral method (Pozrikidis, 1995; Ramanujan and Pozrikidis, 1998), and immersed boundary technique similar to the one presented above (Eggleton and Popel, 1998). Fig. 2a presents the deformed shapes of a capsule after it has reached a steady state. Deformation of the capsule into an ellipsoidal shape, and alignment with the flow direction are evident here. We also show variation in capsule shape with varying capillary numbers. Deformation and alignment increase with increasing capillary number. These results are qualitatively similar to those obtained by Pozrikidis (1995), Ramanujan and Pozrikidis (1998), and Eggleton and Popel (1998). We also present the time-history of capsule orientation by showing the angle that the major axis of the ellipsoid makes with the x direction (Fig. 2b). After an initial transience, the capsule aligns at a steady angle with the flow, and the asymptotic angle decreases with increasing Ca.

Quantitative comparison between the present and previous results is shown in Fig. 2c (inset). Here we show the Taylor deformation parameter D defined as $D = (L - B)/(L + B)$ where L and B are the major and minor axis of the ellipsoid in the plane of the shear. Fig. 2c (inset) shows the time-history of the Taylor deformation for various Ca at $Re \ll 1$. The results obtained from the present method are compared with those of the boundary integral simulations of Ramanujan and Pozrikidis (1998). Excellent agreement between the two can be seen. The steady-state value of D increases with increasing Ca. Sensitivity of our results to the Eulerian resolution is also shown in Fig. 2c by considering two simulations at 80^3 and 120^3 resolutions. No significant difference is observed. Computations using

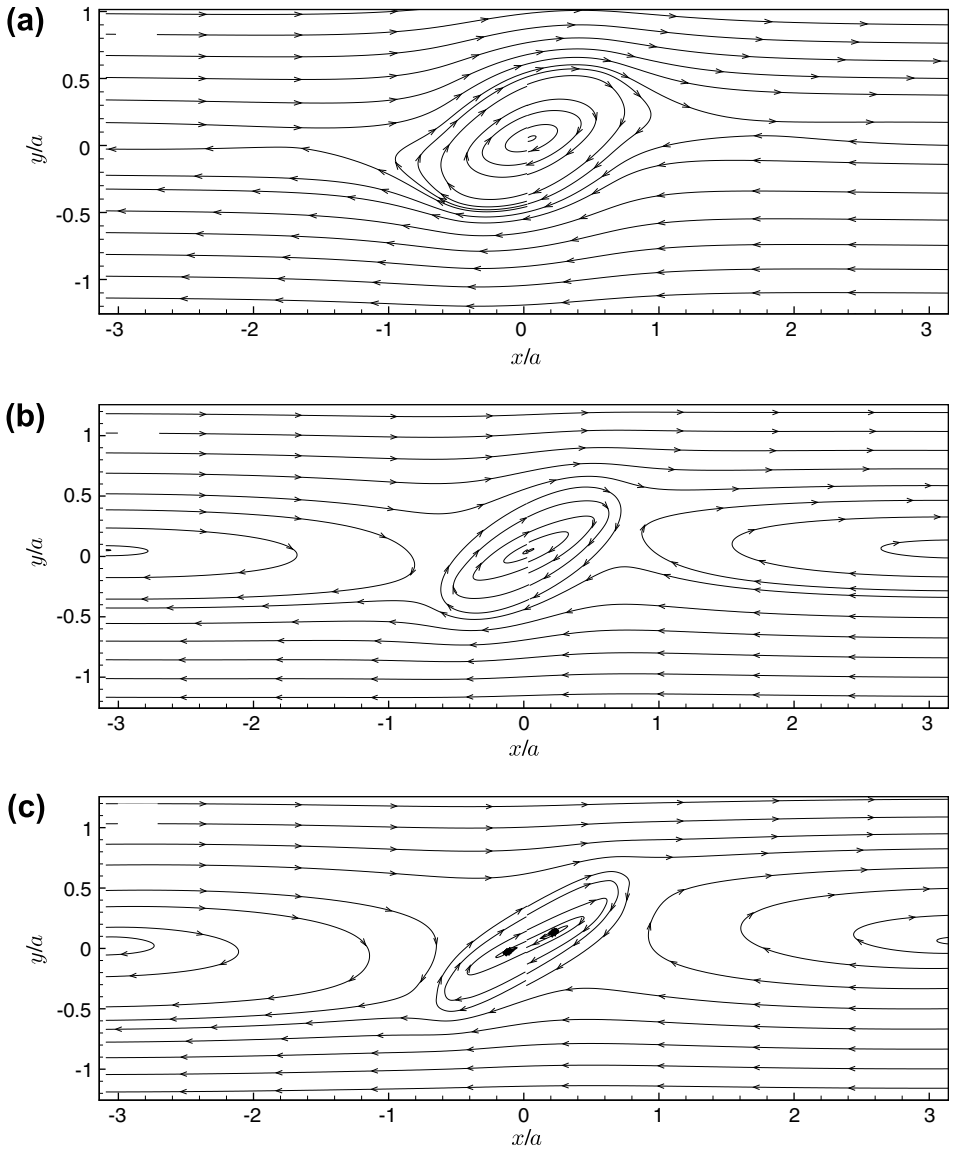

Fig. 4. Flow field around single capsule at (a) $Re \ll 1$, (b) $Re = 10$, and (c) $Re = 50$.

1280 and 5120 triangular elements on the capsule surface also showed no significant difference (data not shown).

3.2. Capsule deformation at finite Re

As mentioned before, previous works on capsule deformation have been mostly limited to $Re \ll 1$. Using the immersed boundary code, we have simulated capsule deformation in shear flow at finite Re up to 50, and We up to 10. The capsule shapes in this range of Re are shown in Fig. 3a. As in the limit of small inertia, capsules at finite inertia also attain a steady ellipsoidal shape and inclined orientation with the flow. We note that the capsule elongates more as Re (or, We) increases. The deformation parameter D and the orientation angle θ are shown in Fig. 3b and c, respectively, with respect to time. The asymptotic steady values of D and θ increase with increasing Re (or, We).

Once the capsule attains the steady deformed shape and orientation, the interior liquid and the membrane rotate in a tank-treading manner. The streamlines in and around the capsule at steady state are shown in Fig. 4 for $Re \ll 1$ and for and $Re = 10$ and 50. For all cases, streamlines within the capsule rotate clockwise in accordance with the direction of vorticity of the imposed flow. The streamlines outside the capsule, however, show significant differences at small and high inertia. For $Re \ll 1$ (Fig. 4a) all streamlines around the capsule extend to infinity. Streamlines in $y/a > 0$ half of the domain go from left to right, and those in $y/a < 0$ go from right to left, in agreement with the imposed shear flow. When Re increases to 10 or 50 (Fig. 4b and c), not all streamlines extend to infinity. Rather, the streamlines within $-0.5 < y/a < 0.5$ form a reverse flow. The streamlines coming from left in $0 < y/a < 0.5$ turn around as they approach the capsule, and then they move to the left in $-0.5 < y/a < 0$. The streamlines coming from right in $-0.5 < y/a < 0$, also turn around as they approach the capsule, and move to the right in $0 < y/a < 0.5$. Between the reverse-flow region, and the capsule, a straining flow region with a off-surface stagnation point is generated. As Re increases from 10 to 50, the reverse-flow region expands more in the lateral (y) direction. Note that the flow domain is periodic in x. Thus we actually simulate an array of capsules with centers located H apart. The reverse streamlines in between two adjacent capsules then form a recirculating flow.

The streamline patters shown here can be compared with those obtained previously for rigid particles suspended in simple shear flow. In the limit of Stokes flow, all streamlines around a rigid spherical or circular particle extends from $-\infty$ to $+\infty$, or vice versa, under a torque-free condition (e.g. Happel and Brenner, 1983; Poe and Acrivos, 1975; Mikulencak and Morris, 2004). At finite inertia, experiments (Poe and Acrivos, 1975) and numerical simulations (Kossack and Acrivos, 1974; Mikulencak and Morris, 2004) have shown the existence of reverse streamlines, and off-surface stagnation points for a torque-free rigid sphere or circular cylinder. The distance between the stagnation points and the center of the particle decreases as Re increases (Poe and Acrivos, 1975). Our results show that the reverse streamlines and off-surface stagnation points also exist for deformable liquid capsules at finite Re.

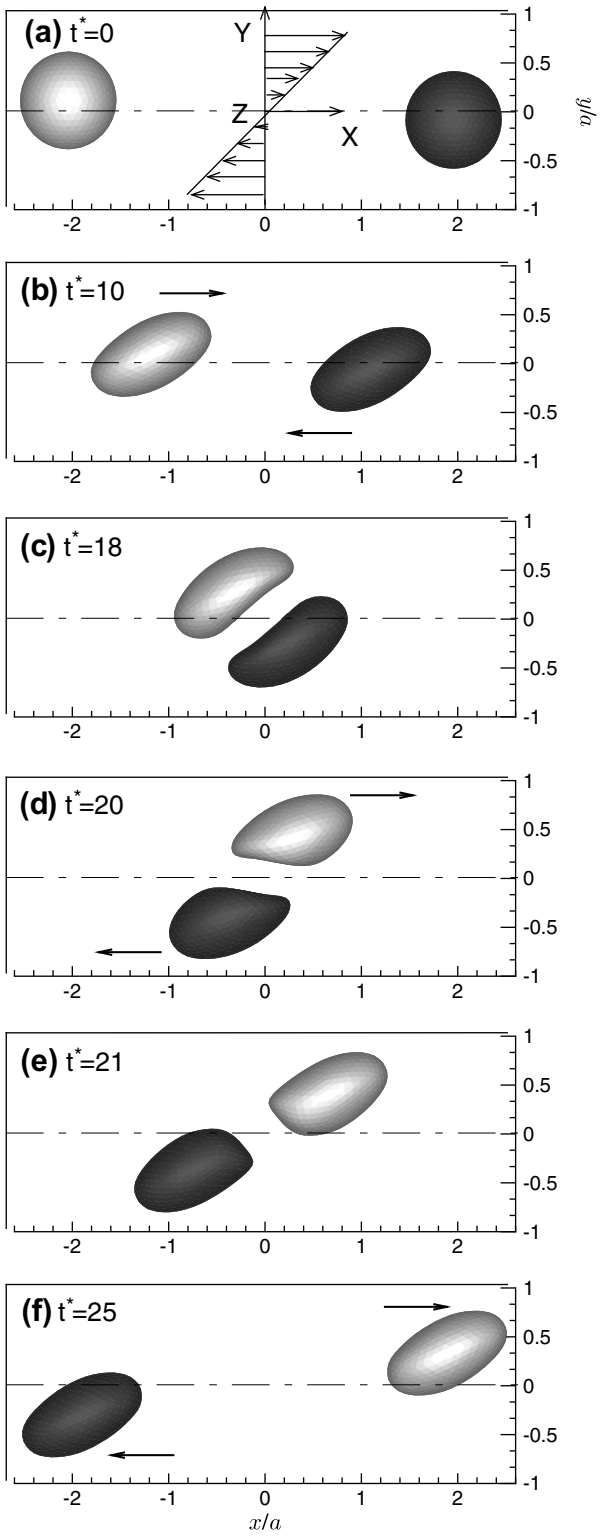

Fig. 5. Sequence of capsule–capsule interaction at $Re \ll 1$. Capsule shapes for $Ca = 0.2$ are shown.

3.3. Capsule–capsule interaction at $Re \ll 1$

Next we consider the main results of the paper, that is, hydrodynamic interaction between two capsules suspended in a shear flow. We first consider the low Re limit, followed by the effect of inertia in the next section. The initial coordinates of the capsule centers are $-x_0$, y_0, z_0, and x_0, $-y_0$, z_0. Thus, the capsules are initially placed off-axis, at small but equal distances above and below the center line at $y = 0$ (Figs. 1b and 5a). The initial lateral and horizontal separations between the centers of the capsules are denoted by Δy_0, and Δx_0. The dimensionless parameter $\Delta y_0/a$ is also called the impact parameter. Due to the non-zero relative velocity between them, the capsules approach each other, and subsequently interact. The sequence of interaction at successive times is shown in Fig. 5 for $Re \ll 1$. Here we consider $Ca = 0.2$, and $\Delta y_0/a = 0.2$, and $\Delta x_0/a = 4$. As the flow starts, the capsules first deform and attain ellipsoidal shapes. As they approach closer, the capsules roll over each other. During the process, both capsules undergo significant deformation, and a flat contact area is formed. Eventually the capsules separate in the x-direction, and the ellipsoidal shapes are recovered. The capsule moving to the right continues to move in that direction, and the one moving to left also continues in that direction.

A close inspection of Fig. 5 reveals that during the interaction, the lateral separation between the capsule first increases and then decreases. The history of the lateral separation Δy between the capsule centroids is shown in Fig. 6. The effect of Ca is also shown here. Δy remains at its initial value of 0.2 until the capsules are close enough. Upon close encounter, Δy increases sharply reaching its maximum when the capsules roll over each other (i.e. $\Delta x \approx 0$). After the interaction, Δy decreases. As the capsules move away from each other, Δy reaches a steady value. The final steady value of Δy ($\approx$0.6) is higher than the initial value of 0.2, implying that the hydrodynamic interaction has resulted in a larger permanent lateral separation between the capsules. The process is irreversible, and in case of a suspension of many particles, such increased displacement during binary collisions collectively leads to the shear-induced diffusion in the system. The binary interaction seen here for the liquid capsules is similar to that recently published by Lac et al. (2007). It is also similar to the binary interaction of non-coalescing liquid drops at zero Reynolds numbers (e.g. Loewenberg and Hinch, 1997) and at finite Reynolds numbers (e.g. Nobari and Tryggvason, 1996), and for rigid particles (e.g. Kromkamp et al., 2005) at finite Re.

3.4. Capsule–capsule interaction at finite Re: short-time behavior

Next we consider the effect of inertia on capsule–capsule interaction. The initial off-sets are $\Delta y_0/a = 0.2$ and $\Delta x_0/a = 4$, same as before. Successive profiles of the capsules are shown in Fig. 7 for $Re = 10$ and $We = 2$. As the flow starts, the capsules deform and attain ellipsoidal shapes. As time progresses, the capsules first approach each other due to the non-zero relative velocity between them (Fig. 7b). As the capsules come closer, however, they do not roll over each other. Rather, they reverse the direction of motion (at $t^* = 12$ in Fig. 7c). The capsule initially moving to the right (shown using light shading) now moves to left, while the one moving to left (shown using dark shading) now moves to right (Fig. 7d). This behavior is remarkably different from that seen earlier at $Re \ll 1$ in Fig. 5, where the capsules rolled over each other, and maintained their respective directions of motion after the interaction. At around $t^* = 28$ (Fig. 7e), the horizontal separation between the capsules is the maximum. At this point, their directions of motion reverse again, and they again start approaching each other, as evident from Fig. 7f for $t^* = 38$. Subsequently, at around $t^* = 45$, the capsules again reverse their motion, and recede from each other (not shown). The simulation was continued for a long time, and the reversal of the motion was observed to repeat continuously.

A number of numerical experiments at finite Re up to 50 are performed. The trajectories of the capsule centroids for different Re are shown in Fig. 8a. We also show the y-coordinates of the capsule centroids versus time in Fig. 8b and c which may also be helpful to describe the capsule interac-

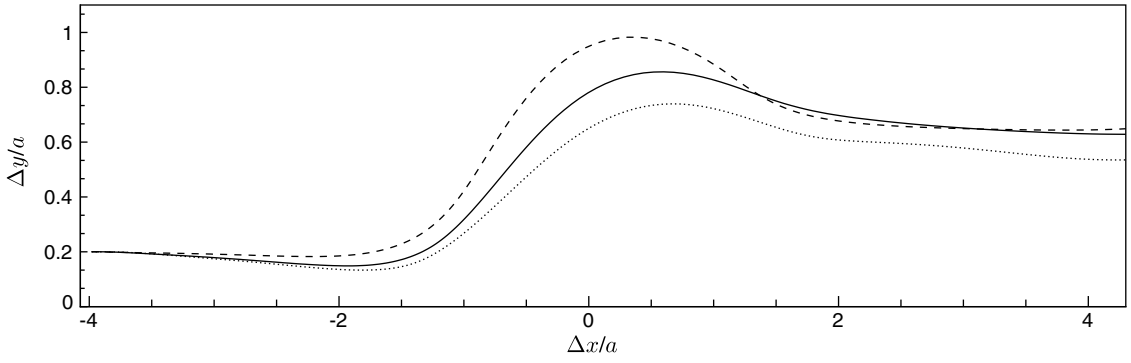

Fig. 6. Lateral separation Δy versus Δx for $Re \ll 1$. Shown here are --- $Ca = 0.05$, — $Ca = 0.2$, $\cdots$ $Ca = 0.4$. t^* increases from left to right. At $t^* = 0$, $\Delta y_0 = 0.2$.

tion at finite Re. For all Re, the initial horizontal separation is 4, and the vertical separation is $\Delta y_0 = 0.2$. The initial locations of the capsule centroids are marked by circles in Fig. 8a. The capsule located in $x < 0$, $y > 0$ initially moves to the right, and the one located in $x > 0$, $y < 0$ moves to the left. Consider first the cases with $Re \ll 1$. The capsules approach each other in nearly horizontal trajectories. As the horizontal separation between them decreases, the capsules roll over each other which results in an increase in the vertical separation between their centers. After the interaction, the capsules move away from each other, and the vertical separation decreases. The capsule initially moving to the right (or left) continues to move in the same direction after the interaction. Next consider $Re = 0.5$. Inertia does not play any significant role at this Re. The trajectories of the capsules at this Re are similar to those obtained for $Re \ll 1$.

Consider next $Re = 1.5$ and 2.3 ($We = 0.075$ and 0.115) in Fig. 8a and b. The effect of inertia is now apparent, as the capsules do not move in horizontal trajectories before the encounter. Rather, they move towards the $y = 0$ axis immediately before the encounter. As a result, the vertical separation between the capsule first decreases. Also note that the capsules move closer to the $y = 0$ axis as Re increases. Upon encounter, the capsules roll over each other. Subsequently, the capsules move away from each other, and continue to maintain their initial direction of motion. Thus the irreversible increase in lateral displacement occurs even at $Re = 1.5$ and 2.3 except that the capsules move laterally towards $y = 0$ axis before the encounter.

When Re increases to 3 (Fig. 8a and c), several remarkable effects of inertia are observed. The capsules first approach each other as before. They also migrate vertically, and move closer towards the $y = 0$ axis. But upon encounter, they do not roll over each other. Rather they reverse their direction of motion upon interaction. The reversal of direction is due to the fact that the capsules cross the $y = 0$ axis. The capsule which is in $y > 0$ before the encounter, moves to $y < 0$ after the encounter, and vice versa. Subsequently, the capsules reverse their direction of motion. The capsule moving to the right (left) before the interaction, moves to the left (right) after the interaction.

When Re increases to 10 and 50, the reversal of motion of the capsules is also observed (Fig. 8a and c). We also note that as Re increases from 3 to 50, the reversal of motion of a capsule happens progressively earlier in time (Fig. 8c).

The interaction between the capsules at finite Re as just described has no similarity in low Re. The irreversible increase in lateral displacement (which leads to the self-diffusion process in case of many particles) observed at low Re is completely absent in presence of moderate to high inertia ($Re > 3$). Recently, Kromkamp et al. (2005) performed numerical simulations of hydrodynamic interaction between two rigid circular cylinders suspended in a simple shear flow in presence of inertia. The Reynolds number of the particles considered in their study ranges from 0.019 to 0.518. At $Re > 0.058$, they observed that the cylinders move vertically towards the $y = 0$ axis before rolling over each other. This result is similar to that obtained by us for three-dimensional and deformable capsules at $Re = 1.5$ and 2.3. These two results therefore suggest that inertia

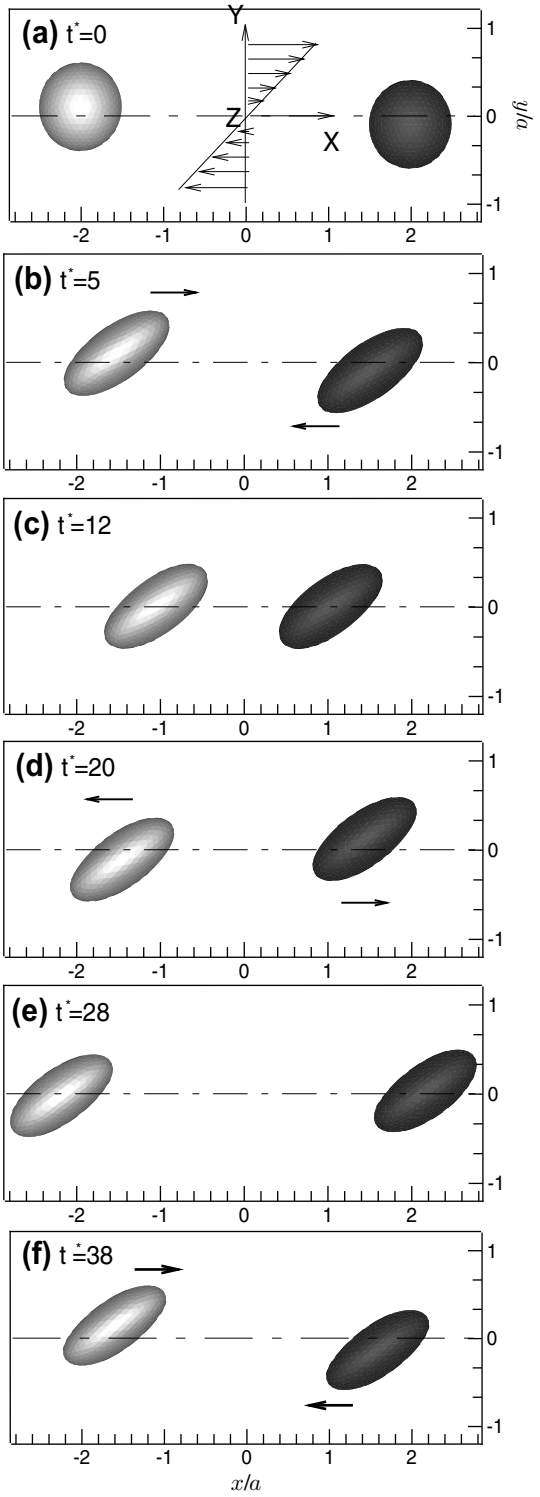

Fig. 7. Sequence of capsule–capsule interaction at finite Re. Shown here is $Re = 10$ ($We = 2$), $\Delta x_0/a = 4$, $\Delta y_0/a = 0.2$.

alters the trajectories of the particles during binary interaction irrespective of whether the bodies are 2D or 3D, and rigid, or deformable. Kromkamp et al. (2005) however, did not consider much higher Reynolds number (e.g. $Re > 1$) as considered in our study. Thus, the reversal of capsule motion for $Re \geqslant 3$ as described above has not been reported by them.

The effect of the impact parameter $\Delta y_0/a$ is studied next in Fig. 9a. We consider $Re = 50$ only, but $\Delta y_0/a = 0.2$, 0.40 and 0.57. Due to the inertia, in all cases, the capsules first approach $y = 0$ axis before encounter. For $\Delta y_0/a = 0.2$ and 0.4, the capsules cross the $y = 0$ axis, and thus reverse their directions of motion. For $\Delta y_0/a = 0.57$, the capsules do not cross the $y = 0$ axis, and they roll over each other, resulting in increased lateral displacement implying shear-diffusion. This result implies that the roll-over or reversal of motion depends on the initial vertical separation (impact parameter), not just on Re (or We). We also note that the reversal of motion occurs earlier as the impact parameter decreases. In the limit $\Delta y_0 \to 0$, there is no interaction between the capsules, and $\Delta x = \Delta x_0$ for all time. In the limit $\Delta y_0 \to \infty$, also there is no interaction between the capsules, and $\Delta y = \Delta y_0$ for all time.

Fig. 9b and c show the effect of Δx_0. Here $\Delta y_0/a$ is held constant at 0.2, and $\Delta x_0/a$ is 1.5 and 8. The Reynolds number considered here is 3, 10, and 50 ($We = 0.15$, 0.5, and 2.5, respectively). For all Re at $\Delta x_0/a = 8$ (Fig. 9b), the capsule trajectories are similar to those obtained for $\Delta x_0/a = 4$ (Fig. 8), and they show the reversal of the capsule motion. Thus, the reversal of the motion is expected to occur even at large $\Delta x_0/a$. On the contrary, capsules with $\Delta x_0/a = 1.5$ (Fig. 9c) show remarkably different trend. In this case, reversal of motion occurs only for $Re = 50$, and the diffusion-type motion (roll-over) occurs for $Re = 3$ and 10.

We now explain the physical reason for the reversal of capsule motion at finite Re. For that, we refer to the

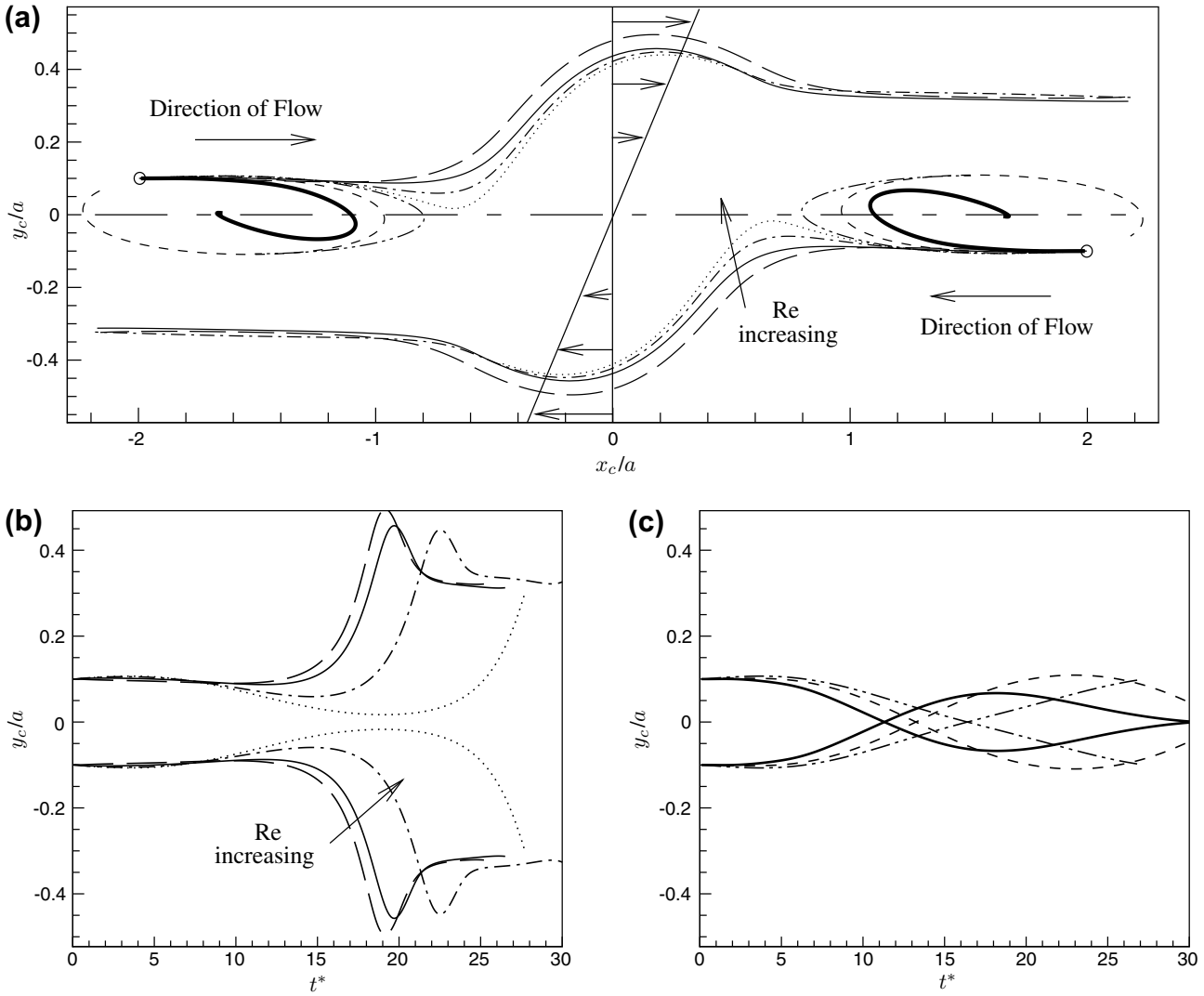

Fig. 8. (a) Capsule trajectories (x_c versus y_c) at finite Re. (b)–(c) lateral coordinates of capsule centroids (y_c) versus t^*. For (a)–(c), line patterns are: ———— $Re \ll 1$; —— $Re = 0.5$; –·–·– $Re = 1.5$; ····· $Re = 2.3$; –··–··– $Re = 3$; ––––– $Re = 10$; thick line $Re = 50$. Symbol 'o' in (a) is the initial location of capsule center.

streamlines plot presented in Fig. 4. It was noted in Fig. 4 that at $Re \ll 1$, the streamlines outside a capsule smoothly follow the deformed shape of the capsule, and extend to ∞. If a second capsule is introduced in the flow, it will follow the streamlines, and move around and over the first capsule as seen in Fig. 5 resulting in self-diffusion type motion. At finite Re, on the other hand, the exterior streamlines near the $y = 0$ axis create a recirculating flow. If a second capsule is released within the recirculating flow, it will follow the closed streamlines, and show the reversal of motion. If it is released outside the recirculating flow, it will follow the open streamlines, and roll over the first capsule. The lateral extent of the recirculating flow increases with increasing Re (Fig. 4). At moderate values of Re (e.g. 1.5 and 2.3 in Fig. 8) and Δy_0 (e.g. 0.2), the initial locations of the capsules are nearly along the boundary of the recirculating flow. Thus the capsule initially move closer to the $y = 0$ axis before rolling over each other. For higher values of Re (>3) but moderate values of Δy_0 (e.g. 0.2 in Fig. 8), the initial locations of the capsules are well within the recirculating flow regions, and hence the capsules reverse their motion. For $Re = 50$ and $\Delta y_0 = 0.57$ (Fig. 9a), the initial locations are outside the reverse flow regions, and hence the capsules roll over each other.

Some more interesting observations at finite Re can be made in Fig. 8b and c, which show the y-coordinate of the capsule centroids versus dimensionless time. First, for $Re < 3$, the time t^* taken by the capsules before they tumble increases with increasing Re. This is because as Re increases, the recirculating flow strengthens, and the vertical component of fluid velocity increases in the recirculating region. The capsules move towards the $y = 0$ axis relatively earlier. As a result, the relative velocity between them (based on the undisturbed shear flow) decreases resulting in longer time before they tumble over each other. For $Re \geqslant 3$, even higher lateral fluid velocity causes the capsules to move quicker towards the $y = 0$ axis, and cross

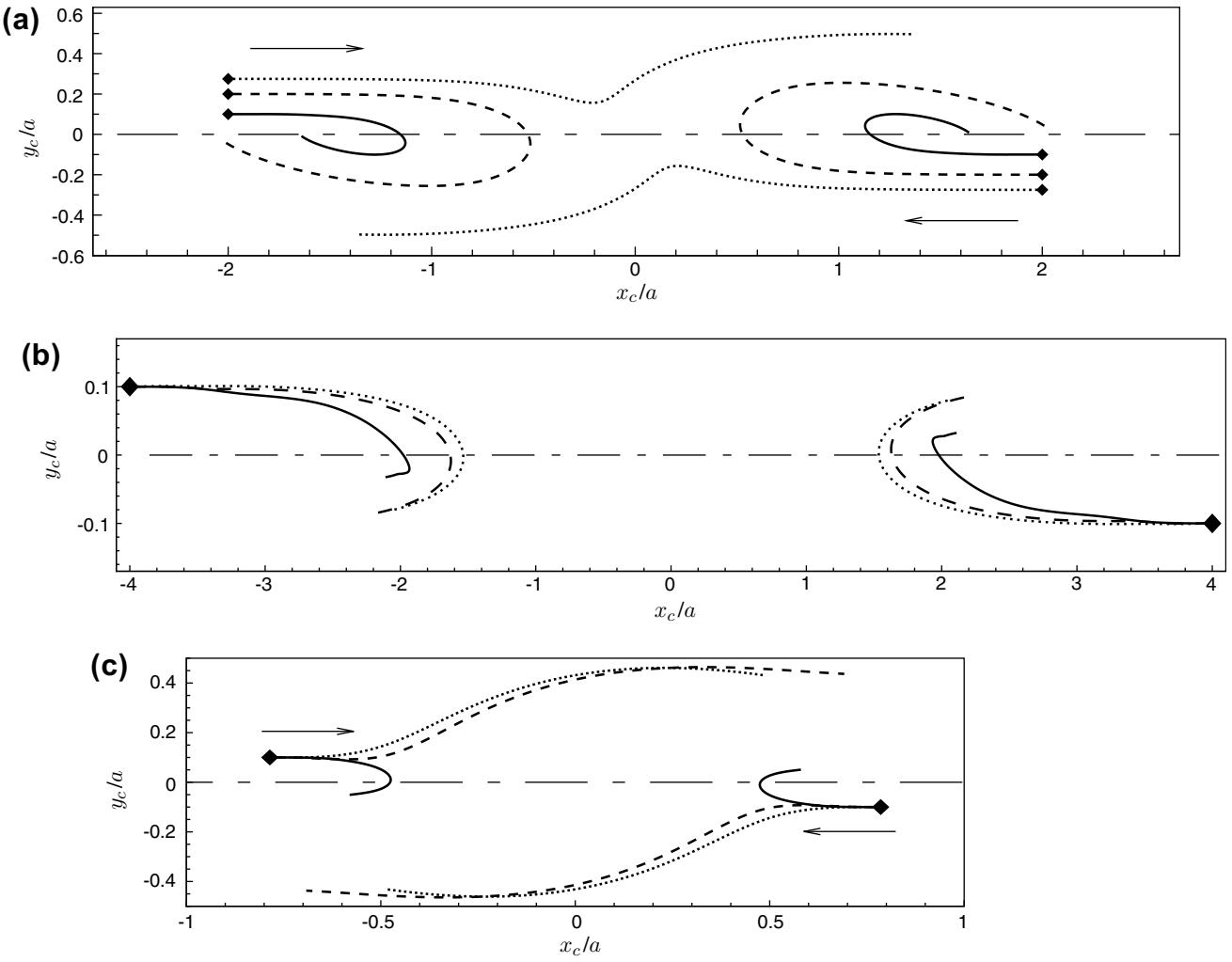

Fig. 9. Capsule trajectories at finite Re. (a) Effect of Δy_0 for $Re = 50$. ····· $\Delta y_0/a = 0.57$; --- $\Delta y_0/a = 0.4$; — $\Delta y_0/a = 0.2$. (b)–(c) Effect of Δx_0. (b) $\Delta x_0 = 8$, and (c) $\Delta x_0 = 1.5$. For (b) and (c) line patterns are: ····· $Re = 3$; --- $Re = 10$; — $Re = 50$. Diamond symbols indicate the initial location of the capsule centroids.

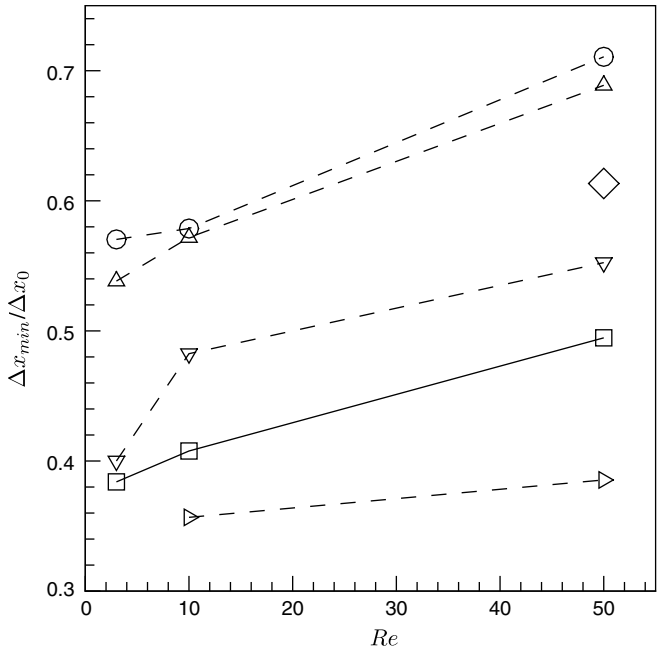

Fig. 10. Minimum horizontal distance between the capsule-pair at finite Re. (□) $\Delta x_0/a = 8$, $\Delta y_0/a = 0.2$; (▷) $\Delta x_0/a = 4$, $\Delta y_0/a = 0.3$; (▽) $\Delta x_0/a = 4$, $\Delta y_0/a = 0.2$; (△) $\Delta x_0/a = 4$, $\Delta y_0/a = 0.1$; (○) $\Delta x_0/a = 4$, $\Delta y_0/a = 0.05$; (◇) $\Delta x_0/a = 1.5$, $\Delta y_0/a = 0.2$.

the axis due to inertia. Thus for $Re \geqslant 3$, the reversal of capsule motion occurs earlier in time with increasing Re. It also implies, as evident from Figs. 8 and 9, that with increasing Re ($\geqslant 3$) the capsules come less closer to each other.

The reversal of the capsule motion should not be confused with the bouncing collision that is often encountered during head-on collision of liquid drops (see, e.g. Nobari and Tryggvason, 1996; Mohamed-Kassim and Longmire, 2004). In the latter case, the drops come close to each other before bouncing. In the present case, the capsules at finite inertia do not come close to each other as evident from Figs. 7. To illustrate this point, we compute the minimum horizontal distance $\Delta x_{\min}$ between the capsules as shown in Fig. 10. We note that $\Delta x_{\min}$ depends on Re, Δx_0 and Δy_0. For a given Δy_0, we see that $\Delta x_{\min}$ increases with increasing Re (also see Fig. 9a), due to the increasing strength of the recirculating flow. For a given Re, $\Delta x_{\min}$ increases with decreasing Δy_0. In the limits $\Delta y_0 \to 0$ or ∞, no interaction can take place, and $\Delta x = \Delta x_0$.

One implication of the fact that the capsules do not come close to each other at finite Re is that the deformed ellipsoidal shapes of the capsules remain unchanged during the interaction. This is in contrast to the observation at low

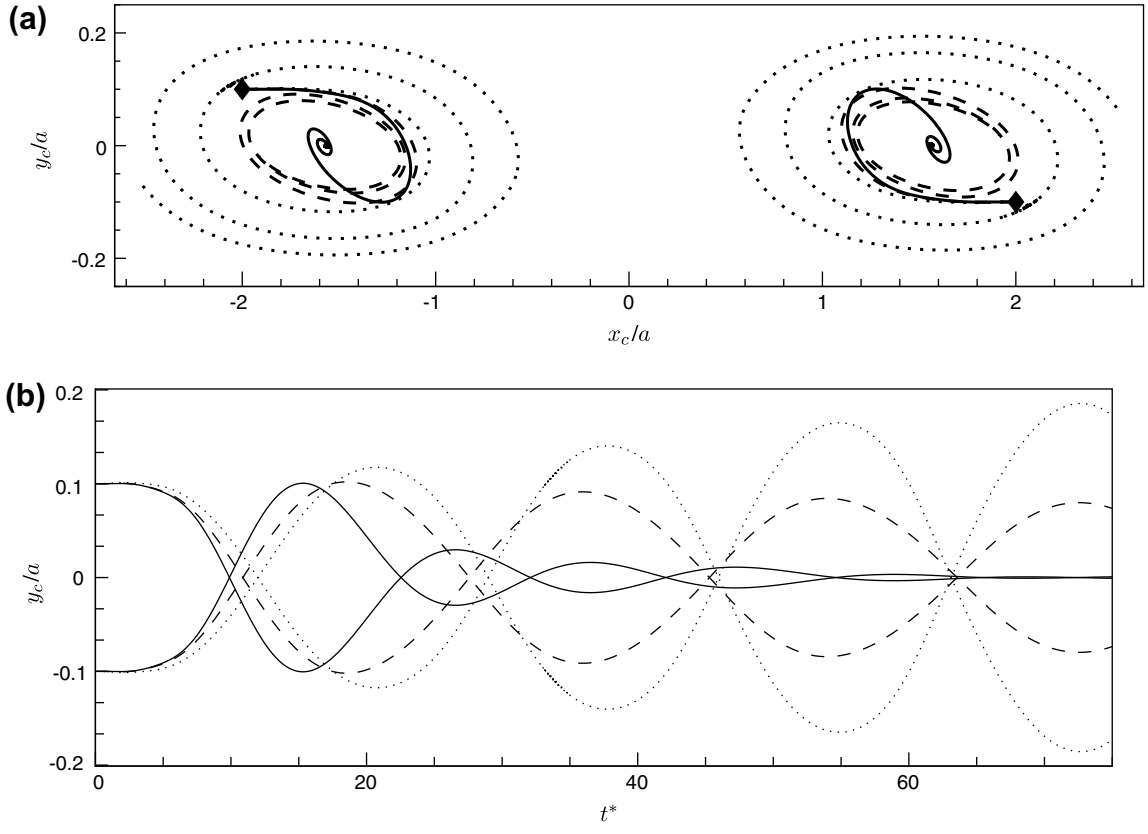

Fig. 11. Long-time trajectories of capsules at finite Re. Line patterns are: ··· $Re = 10$, --- $Re = 25$, — $Re = 50$. Diamond symbols indicate the initial capsule locations.

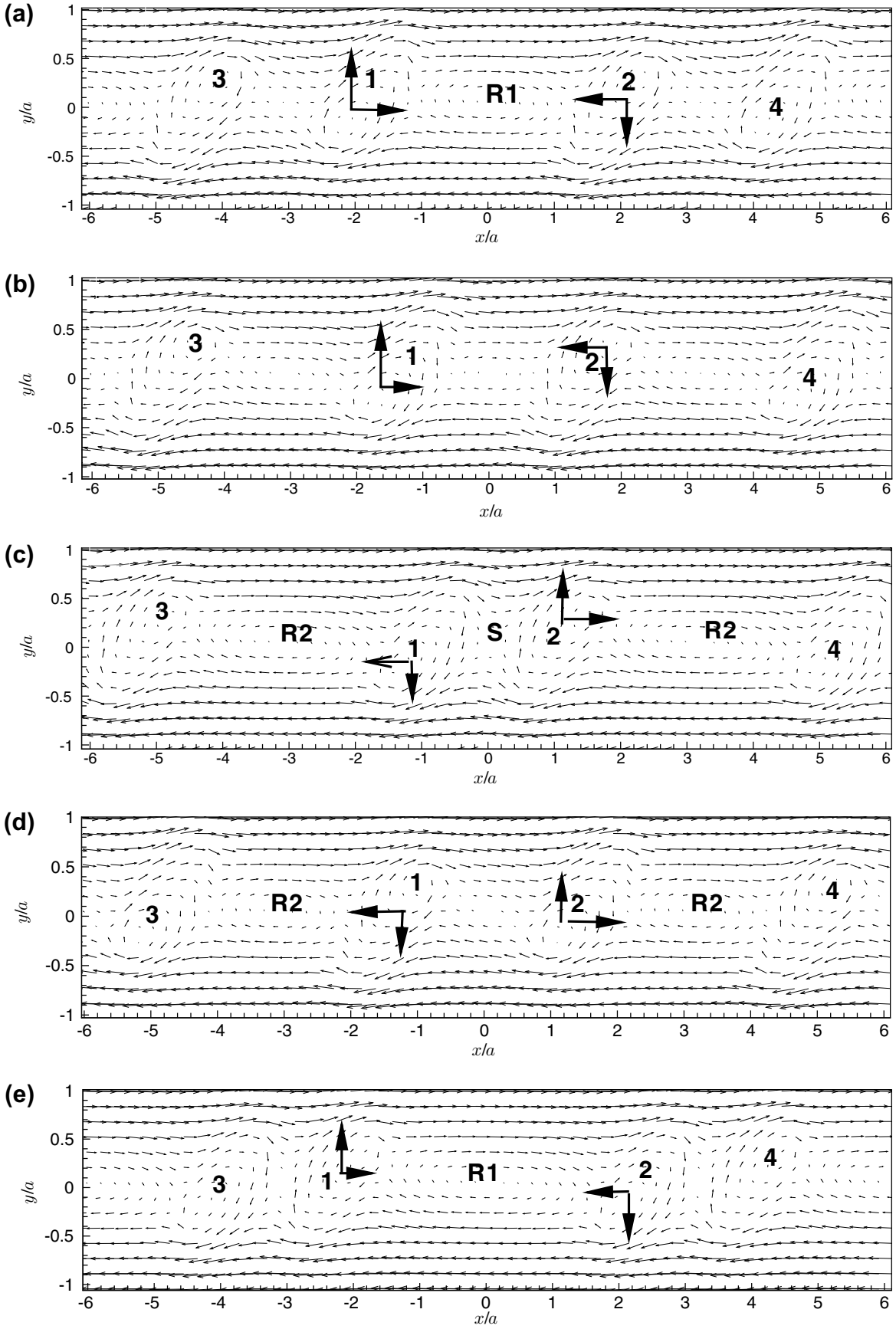

Fig. 12. Time sequence of fluid velocity vectors for capsule–capsule interaction at $Re = 10$. (a)–(e) are at $t^* = 5$, 9, 12, 20, and 28.

Re, where capsule shapes deform significantly during the interaction (Fig. 5).

3.5. Capsule–capsule interaction at finite Re: long-time behavior

So far we discussed the results on the first encounter between the capsules. Simulations presented above were continued for longer time. We now discuss the long-time behavior of the capsules. For this we only consider the cases for which reversal of capsule motion was observed. The long-time behavior can be illustrated by going back to Fig. 7. Here we see that the capsules, after deforming, first approach each other, then recede from each other (at $t^* \approx 12$–28), and then again approach each other (at $t^* \approx 28$–38). They also periodically move above and below the $y = 0$ axis. The periodic approach and receding motion continued throughout the length of the simulation ($t^* \approx 100$). Simulations at higher *Re* and *We* also show similar periodic motion, details of which are described later. Such periodic approach and receding motion over long time at high *Re* has no similarity at low *Re*.

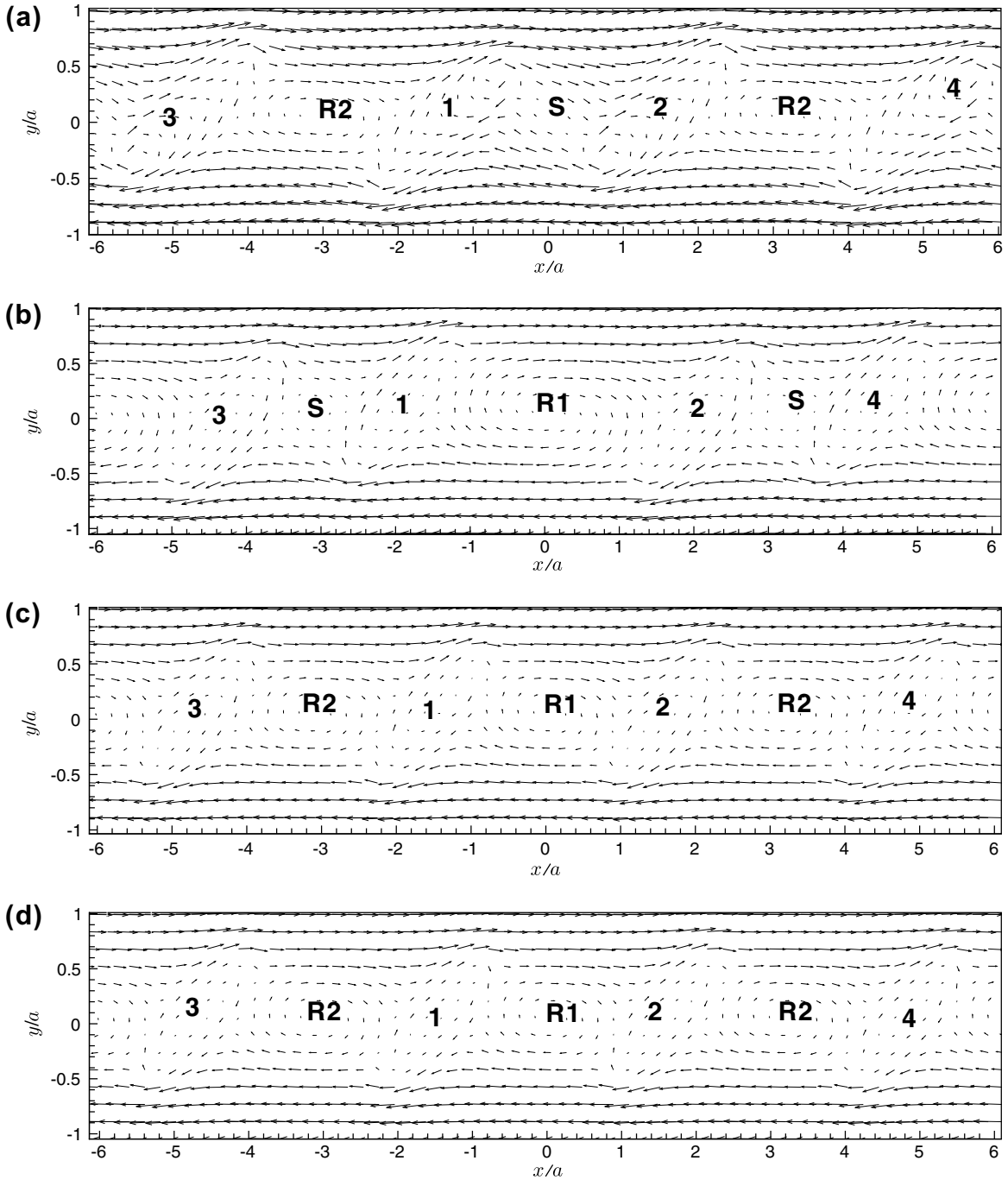

Fig. 13. Same as in previous figure but for $Re = 50$. (a)–(d) are at $t^* = 18$, 23, 28, and 33.

Long-time trajectories of the capsules for $Re = 10$, 25 and 50 ($We = 2$, 5 and 10, respectively) are shown in Fig. 11. The trajectories show that the capsules move in spirals, and thus repeatedly approach and recede. The direction of the spiraling motion coincides with the direction of the vorticity of the imposed shear flow. The trajectories do not show the same behavior for all Re and We. At $Re = 10$, the capsules move spirally outward. At $Re = 25$, the capsules first spiral inward, but eventually continue to spiral in fixed orbits. At $Re = 50$, the capsules spiral inward, and then settle on the $y = 0$ axis after which no significant motion of them is observed. The spiraling motion of the capsules is further illustrated in Fig. 11b showing the capsule centroids (y_c) versus t^*. For both capsules y_c oscillates about $y = 0$. For $Re = 10$, amplitude of oscillations increases with time as is the case for an outward spiral. For $Re = 25$, the amplitude remains constant as is the case for a fixed-orbit motion. For $Re = 50$, oscillations are damped as the capsules spiral inward and eventually settle at $y = 0$ axis.

The explanation for the different spiraling motions (outward, inward or fixed-orbit) can again be based on the existence of the recirculating flow formed in between two adjacent capsules in an array (Fig. 4). The explanation is given using the fluid velocity vectors shown in Figs. 12 and 13 where two pairs of capsules are considered since the flow is periodic in x. The capsules are marked by number 1, 2 etc. Consider $Re = 10$ first in Fig. 12. At $t^* = 5$ (Fig. 12a), a recirculating flow exists (marked by 'R1' in the figure) between the capsules 1 and 2 where the fluid moves in the clockwise direction. At this moment the centers of capsules 1 and 2 are located above and below $y = 0$, respectively. As the capsules approach each other, the recirculating flow between them weakens. At $t^* \approx 12$ (Fig. 12c), the capsules are closest to each other, and the recirculating flow between them is absent. Instead, a straining flow region exists (marked by 'S' in Fig. 12c). The generation of this straining flow region was also discussed in section III-B. At this point, however, two recirculating regions, marked by 'R2' in Fig. 12c, develop between capsules 3 and 1, and between 2 and 4. As a result, capsule 1 now starts moving downward towards $y = 0$, and capsule 2 moves upward towards $y = 0$. Due to inertia, the capsules cross the $y = 0$ axis. Once the capsule 1 is in $y < 0$, and capsule 2 is in $y > 0$, they start receding from each other (Fig. 12d). The intercapsule gap between 1 and 2 starts increasing and a recirculating flow re-emerges there (marked by 'R1' in Fig. 12e), whereas straining flow regions re-emerges between 3 and 1, and between 2 and 4. The cycle is then repeated.

The vector plots for $Re = 50$ are shown in Fig. 13. As noted earlier in Fig. 4 for single capsule, the off-surface stagnation points are located closer to the capsule as Re increases. As a result, the recirculating flow develops between two capsules even when the inter-capsule gap is relatively small. The effect from two adjacent recirculating regions is nullified by each other, and eventually the capsules attain a stable position at $y = 0$ axis.

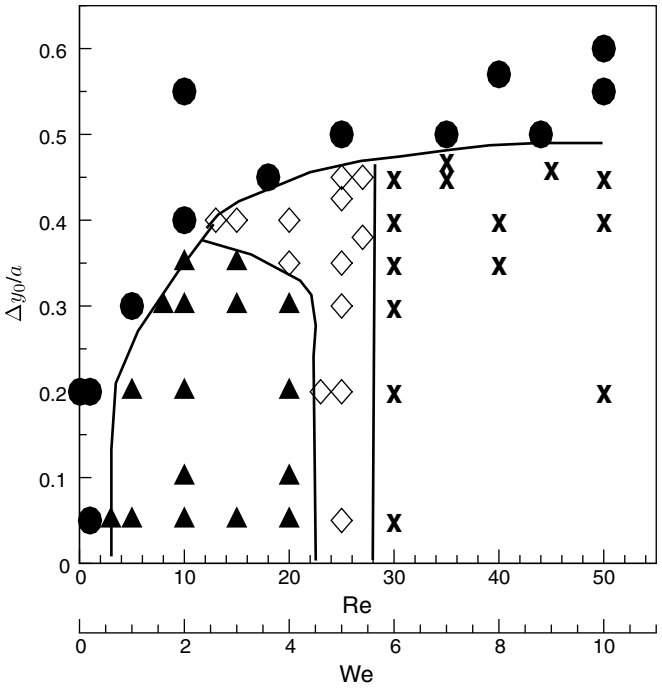

Fig. 14. Regimes of capsule–capsule interaction at finite Re and We. ●, Self-diffusion type motion; ▲, outward spiraling motion; × inward spiraling motion; and ◇, fixed-orbit motion.

3.6. Regimes of capsule–capsule interaction at finite Re

Above results suggest that increased lateral displacement upon binary interaction, which is characteristic of $Re \ll 1$, may or may not be present at finite Re (or, We) depending on the impact parameter $\Delta y_0/a$ and the initial gap $\Delta x_0/a$. In the case where such interaction is present, the lateral separation between the capsules first decreases before they roll over each other. In the case when such interaction is absent, the capsule-pair engages in a spiraling motion. The spiraling motion could be either outward, inward or fixed-orbit. These regimes of motion are shown in a Re–Δy_0 (or, We–Δy_0) plane in Fig. 14 for a fixed $\Delta x_o/a = 4$. Based on the computational results, four different regimes in capsule–capsule interaction at finite Re can be identified. They are: (i) a self-diffusive type interaction for $Re < 3$ ($We < 1$) and any Δy_0 in which the capsules roll over each other as in case of $Re \ll 1$, (ii) an outwardly spiraling motion for $3 < Re < 20$ ($1 < We < 4$) and for low values of $\Delta y_0/a$ (<0.4), (iii) a fixed-orbit spiraling motion for $20 < Re < 30$ ($4 < We < 6$) and $\Delta y_0/a < 0.4$, and (iv) an inwardly spiraling motion for $Re > 30$ ($We > 6$) and $\Delta y_0/a < 0.4$ in which the capsules settle at $y = 0$.

4. Summary and conclusion

Three-dimensional numerical simulations using front-tracking method are performed to study the dynamics of deformable liquid capsules in simple shear flow. Capsules are modeled as liquid drops surrounded by neo-Hookean

elastic membranes. Comparison of the results on large deformation of capsules obtained using the present methodology and previous boundary integral simulations showed excellent agreement. The main objective of this article was to study the effect of inertia on the hydrodynamic interaction between a pair of capsules. In the limit of zero inertia, it has been known from past research that the hydrodynamic interaction between two deformable particles (drops/capsules) suspended in shear flow with a relative velocity results in an irreversible shift in the trajectories of the particles leading to the so-called shear-induced diffusion, in case of a suspension of many particles. In this article we investigated the effect of inertia on the deformation of single capsule, and on capsule–capsule interaction. Throughout the article, we draw comparison between the results at finite inertia and at small inertia. The main results from this study are summarized below.

1. At finite inertia, a capsule in a shear flow deforms in to an ellipsoidal shape, and deformation increases with increasing Re. The flow field around a capsule showed reverse flow regions and off-surface stagnation points, similar to those previously reported in case of torque-free spheres and cylinders. The lateral extent of the reverse flow increases with increasing Re.
2. The present methodology has been successful to simulate the irreversible trajectory shift resulting from the hydrodynamic interaction between two liquid capsules at $Re \ll 1$. Similar to liquid drops, capsules at $Re \ll 1$ undergo irreversible increase in their lateral separation implying the possibility of the shear-induced diffusion mechanism in case of a capsule suspension. During the interaction, the capsules undergo significant deformation. To the best of our knowledge, apart from the present study, there is only one study that addressed the binary interaction of liquid capsules (Lac et al., 2007).
3. Effect of inertia on the interaction between two capsules is quite remarkable. For $1 < Re < 3$, the capsules do undergo increased lateral displacement, but their trajectories are different from those at $Re \ll 1$. Specifically, the lateral separation between the capsules first decreases before they roll over each other. For $Re > 3$, the capsules reverse their directions of motion before coming close to each other. Thus, for $Re > 3$, the shear-induced diffusion can be absent. The reversal of the capsule motion is explained based on the recirculating streamlines formed around the capsule at finite Re. The reversal of motion occurs progressively earlier in time (that is, the capsules come less closer to each other) with increasing Re.
4. The long-time behavior of the capsule–capsule interaction at finite inertia showed that the capsules engage in spiraling motions. The nature of the spiraling motion depends on Re and We, and the initial separation between the capsules. The spiraling motion of the capsules is also explained based on the recirculating streamlines formed around the capsule at finite Re.
5. Based on our simulations, four different regimes of capsule–capsule interaction at finite inertia are identified: (i) a self-diffusive type interaction for $Re < 3$ ($We < 1$), (ii) an outwardly spiraling motion for $3 < Re < 20$ ($1 < We < 4$), (iii) a fixed-orbit spiraling motion for $20 < Re < 30$ ($4 < We < 6$), and (iv) an inwardly spiraling motion for $Re > 30$ ($We > 6$) in which the capsules settle with zero relative velocity. These spiraling motions at finite Re have no analogy at $Re \ll 1$.

One distinct feature of capsule–capsule interaction at finite inertia is that the capsules do not come close enough so that the interaction does not lead to further deformation of them. This is in stark contrast to $Re \ll 1$ limit when the capsules undergo significant deformation during the interaction. These, and other results presented here may have implications in developing a theory of capsule suspension. By considering the binary interaction of capsules, this study forms the basis of addressing the more difficult problem of suspension of deformable capsules or other deformable particles at finite inertia.

It should be noted that the results presented here are in a domain bounded in the velocity gradient direction, and periodic in other two directions. While different trajectories are obtained depending on the particle Reynolds number, the effect of the bounding wall certainly plays a role. In order to assess the wall effect, one needs to consider either open boundaries in the velocity gradient direction, or at least, consider a large channel height to particle size ratio. In this article we have not pursued this. A recent work by Zurita-Gotor et al. (2007) indeed showed that swapping trajectories are possible even in the limit of Stokes flow when a bounded domain is considered. It appears that the interplay of wall effects and inertia presents rich physics and an interesting area of further research.

Further, for the highest capsule Re considered here, and given the channel width to capsule size ratio, the Reynolds number based on the channel width ($Re_H = GH^2/\nu$) is 1953. A plane Couette flow is linearly stable for all Re_H, whereas it becomes unstable to spanwise disturbance in the range 600–800 (see, e.g. Barkley and Tuckerman, 1999). In our code, we do not observe such instability unless we enforce 3D disturbance.

In closing, we emphasize that the results presented here are for capsule pairs moving in the shear plane. For a general understanding of a suspension, off-plane interactions would also be important which are left for future investigation.

Computations are performed on the IBM p690 at the National Center for Supercomputing Applications at University of Illinois at Urbana-Champaign.

References

Acrivos, A., Batchelor, G.K., Hinch, E.J., Koch, D.L., Mauri, R., 1992. Longitudinal shear-induced diffusion of spheres in a dilute suspension. J. Fluid Mech. 240, 651–657.

Ashgriz, N., Poo, J.Y., 1990. Coalescence and separation in binary collisions of liquid drops. J. Fluid Mech. 221, 183–204.

Barkley, D., Tuckerman, L.S., 1999. Stability analysis of perturbed plane Couette flow. Phys. Fluids 11, 1187–1195.

Barthes-Biesel, D., 1980. Motion of a spherical microcapsule freely suspended in a linear shear flow. J. Fluid Mech. 100, 831–853.

Barthes-Biesel, D., Chim, V., 1981. Constitutive equation of a dilute suspension of spherical microcapsules. Int. J. Multiphase Flow 7, 473–493.

Barthes-Biesel, D., Rallison, J.M., 1981. The time-dependent deformation of a capsule freely suspended in a linear shear flow. J. Fluid Mech. 113, 251–267.

Barthes-Biesel, D., Sgaier, H., 1985. Role of membrane viscosity in the orientation and deformation of a spherical capsule suspended in shear flow. J. Fluid Mech. 160, 119–135.

Barthes-Biesel, D., Diaz, A., Dhenin, E., 2002. Effect of constitutive laws for two-dimensional membranes on flow-induced capsule deformation. J. Fluid Mech. 460, 211–222.

Batchelor, G.K., Green, J.T., 1972. The hydrodynamic interaction of two small freely-moving spheres in a linear flow field. J. Fluid Mech. 56, 375–400.

Borhan, A., Gupta, N.R., 2003. Capsule motion and deformation in tube and channel flow. In: Pozrikidis, C. (Ed.), Modeling and Simulation of Capsules and Biological Cells. Chapman & Hall/CRC, Boca Raton, Florida.

Brady, J.F., Bossis, G., 1985. The rheology of concentrated suspensions of spheres in simple shear flow by numerical simulation. J. Fluid Mech. 155, 105–129.

Brady, J.F., Morris, J.F., 1997. Microstructure of strongly sheared suspensions and its impact on rheology and diffusion. J. Fluid Mech. 348, 103–139.

Breedveld, V., van den Ende, D., Tripathi, A., Acrivos, A., 1998. The measurement of the shear-induced particle and fluid tracer diffusivities in concentrated suspensions by a novel method. J. Fluid Mech. 375, 297–318.

Breedveld, V., van den Ende, D., Bosscher, M., Jongschaap, R.J.J., Mellema, J., 2001. Measuring shear-induced self-diffusion in a counterrotating geometry. Phys. Rev. E 63, 021403.

Brenn, G., Kolobaric, V., 2006. Satellite droplet formation by unstable binary drop collisions. Phys. Fluids 18, 087101.

Breyiannis, G., Pozrikidis, C., 2000. Simple shear flow of suspensions of elastic capsules. Theor. Comput. Fluid Dynamics 13, 327–347.

Chang, K.S., Olbricht, W.L., 1993. Experimental studies of the deformation of a synthetic capsule in extensional flow. J. Fluid Mech. 250, 587–608.

Chang, C., Powell, R.L., 1994. Self-diffusion of bimodal suspensions of hydrodynamically interacting spherical particles in shearing flow. J. Fluid Mech. 281, 51–80.

Charles, R., Pozrikidis, C., 1998. Significance of the dispersed-phase viscosity on the simple shear flow of suspensions of two-dimensional liquid drops. J. Fluid Mech. 365, 205–233.

Charrier, J.M., Shrivastava, S., Wu, R., 1989. Free and constrained inflation of elastic membranes in relation to thermoforming-non-axisymmetric problems. J. Strain Anal. 24, 55–74.

daCunha, F.R., Hinch, E.J., 1996. Shear-induced dispersion in a dilute suspension of rough spheres. J. Fluid Mech. 309, 211–223.

Darabaner, C.L., Mason, S.G., 1967. Particle motion in sheared suspension. XXII. Interactions of rigid spheres (Experimental). Rheol. Acta 6, 273.

Diaz, A., Pelekasis, N., Barthes-Biesel, D., 2000. Transient response of a capsule subjected to varying flow conditions: effect of internal fluid viscosity and membrane elasticity. Phys. Fluids 12, 948–958.

Diaz, A., Barthes-Biesel, D., Pelekasis, N., 2001. Effect of membrane viscosity on the dynamic response of an axisymmetric capsule. Phys. Fluids 13, 3835–3839.

Drazer, G., Koplik, J., Khusid, B., Acrivos, A., 2002. Deterministic and stochastic behavior of non-Brownian spheres in sheared suspensions. J. Fluid Mech. 460, 307–335.

Eckstein, E.C., Bailey, D.G., Shapiro, A.H., 1977. Self-diffusion of particles in shear flow of a suspension. J. Fluid Mech. 79, 191–208.

Eggleton, C.D., Popel, A.S., 1998. Large deformation of red blood cell ghosts in a simple shear flow. Phys. Fluids 10, 1834–1845.

Foss, D.R., Brady, J.F., 1999. Self-diffusion in sheared suspensions by dynamic simulation. J. Fluid Mech. 401, 243–274.

Guido, S., Simeone, M., 1998. Binary collisions of drops in simple shear flow by computer-assisted video optical microscopy. J. Fluid Mech. 357, 1–20.

Gutcho, M.H., 1979. Microcapsules and other Capsules. Noyes Data Corporation, Park Ridge, NJ.

Happel, J., Brenner, H., 1983. Low Reynolds Number Hydrodynamics. Kluwer.

Kossack, C.A., Acrivos, A., 1974. Steady simple shear flow past a circular cylinder at moderate Reynolds numbers: a numerical solution. J. Fluid Mech. 66, 353–376.

Kromkamp, J., Van den Ende, D.T.M., Kandhai, D., Van der Sman, R.G.M., Boom, R.M., 2005. Shear-induced self-diffusion and microstructure in non-Brownian suspensions at non-zero Reynolds numbers. J. Fluid Mech. 529, 253–278.

Kwak, S., Pozrikidis, C., 2001. Effect of membrane bending stiffness on the axisymmetric deformation of capsules in uniaxial extensional flow. Phys. Fluids 13, 1234–1244.

Lac, E., Barthes-Biesel, D., 2005. Deformation of a capsule in simple shear flow: Effect of membrane prestress. Phys. Fluids 17, 072105.

Lac, E., Barthes-Biesel, D., Pelekasis, N.A., Tsamopoulos, J., 2004. Spherical capsules in three-dimensional unbounded Stokes flows: effect of the membrane constitutive law and onset of buckling. J. Fluid Mech. 516, 303–334.

Lac, E., Morel, A., Barthes-Biesel, D., 2007. Hydrodynamic interaction between two identical capsules in simple shear flow. J. Fluid Mech. 573, 149–169.

Leighton, D.T., Acrivos, A., 1987. Measurement of shear-induced self-diffusion in a concentrated suspension of spheres. J. Fluid Mech. 177, 109–131.

Leyrat-Maurin, A., Barthes-Biesel, D., 1994. Motion of a deformable capsule through a hyperbolic constriction. J. Fluid Mech. 279, 135–163.

Li, X.Z., Barthes-Biesel, D., Helmy, A., 1988. Large deformations and burst of a capsule freely suspended in an elongational flow. J. Fluid Mech. 187, 179–196.

Loewenberg, M., Hinch, E.J., 1997. Collision of two deformable drops in shear flow. J. Fluid Mech. 338, 299–315.

Marchioro, M., Acrivos, A., 2001. Shear-induced particle diffusivities from numerical simulations. J. Fluid Mech. 443, 101–128.

Mikulencak, D.R., Morris, J.F., 2004. Stationary shear flow around fixed and free bodies at finite Reynolds number. J. Fluid Mech. 520, 215–242.

Mohamed-Kassim, Z., Longmire, E.K., 2004. Drop coalescence through a liquid/liquid interface. Phys. Fluids 16, 2170–2183.

Nobari, M.R.H., Tryggvason, G., 1996. Numerical simulations of three dimensional drop collisions. AIAA J. 34, 750–755.

Pan, Y., Suga, K., 2005. Numerical simulation of binary liquid droplet collision. Phys. Fluids 17, 082105.

Pigeonneau, F., Feuillebois, F., 2002. Collision of drops with inertia effects in strongly sheared linear flow fields. J. Fluid Mech. 455, 359–386.

Poe, G.G., Acrivos, A., 1975. Closed-streamline flows past rotating single cylinders and spheres: inertia effects. J. Fluid Mech. 72, 605–623.

Pozrikidis, C., 1995. Finite deformation of liquid capsules enclosed by elastic membranes in simple shear flow. J. Fluid Mech. 297, 123–152.

Pozrikidis, C., 2001. Effect of membrane bending stiffness on the deformation of capsules in simple shear flow. J. Fluid Mech. 440, 269–291.

Pozrikidis, C., 2003. Modeling and Simulation of Capsules and Biological Cells. Chapman & Hall/CRC, Boca Raton, FL.

Qian, J., Law, C.K., 1997. Regimes of coalescence and separation in droplet collision. J. Fluid Mech. 331, 59–80.

Queguiner, C., Barthes-Biesel, D., 1997. Axisymmetric motion of capsules through cylindrical channels. J. Fluid Mech. 348, 349–376.

Ramanujan, S., Pozrikidis, C., 1998. Deformation of liquid capsules enclosed by elastic membranes in simple shear flow: large deformations and the effect of fluid viscosities. J. Fluid Mech. 361, 117–143.

Risso, F., Colle-Paillot, F., Zagzoule, M., 2006. Experimental investigation of a bioartificial capsule flowing in a narrow tube. J. Fluid Mech. 547, 149–174.

Roisman, I.V., 2004. Dynamics of inertia dominated binary drop collisions. Phys. Fluids 16, 3438–3444.

Sierou, A., Brady, J.F., 2004. Shear-induced self-diffusion in non-colloidal suspensions. J. Fluid Mech. 506, 285–314.

Unverdi, S.O., Tryggvason, G., 1992. A front-tracking method for viscous, incompressible multi-fluid flows. J. Comput. Phys. 100, 25–37.

Wang, H.W., Zinchenko, A., Davis, R.H., 1994. The collision rate of small drops in linear flow fields. J. Fluid Mech. 265, 161–188.

Wang, Y., Mauri, R., Acrivos, A., 1996. The transverse shear-induced liquid and particle tracer diffusivities of a dilute suspension of spheres undergoing a simple shear flow. J. Fluid Mech. 327, 255–272.

Zurita-Gotor, M., Blawzdziewicz, J., Wajnryb, E., 2007. Swapping trajectories: a new wall-induced cross-streamline particle migration mechanism in a dilute suspension of spheres. J. Fluid Mech. 592, 447–469.